Table of content

1 Characterization of 1,1,2,2-tetrakis(4-phosphonophenyl)ethylene

The linker molecule 1,1,2,2-tetrakis(4-phosphonophenyl)ethylene was synthesized as described in literature.[1] The ^{1}H- and ^{31}P-NMR spectra of the final product are shown in Fig. S1 and S2.

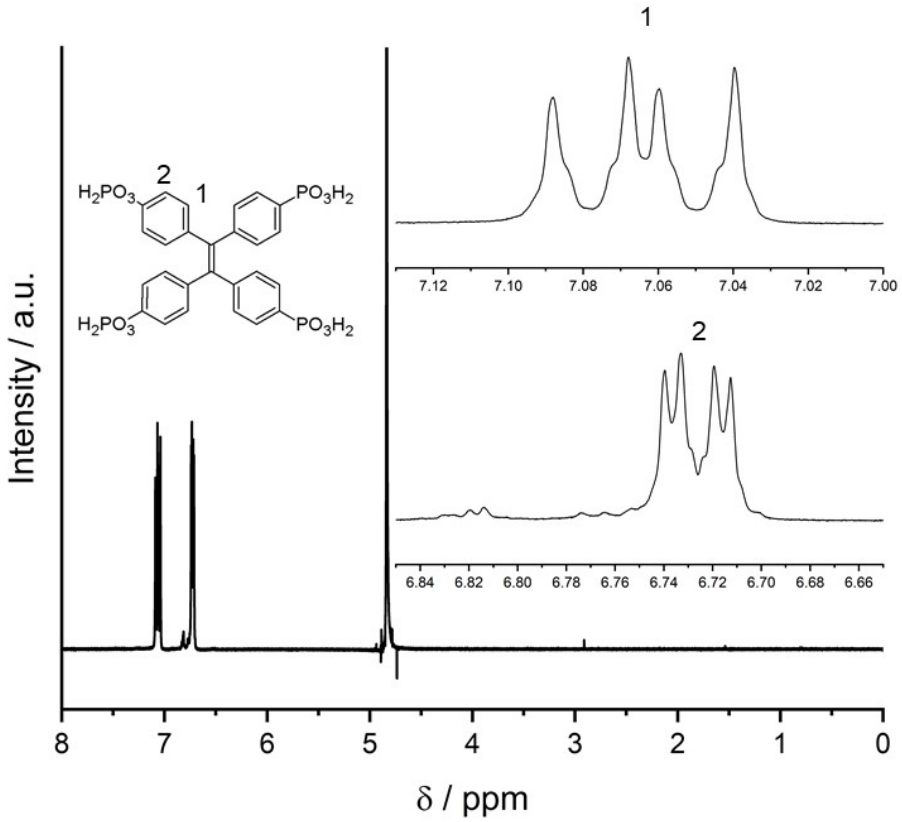

Fig. S1 ^{1}H-NMR-spectrum of 1,1,2,2-tetrakis(4-phosphonophenyl)ethylene.

^{1}H-NMR (400 MHz, 300 K, NaOD/D_2O (10 %)): δ=7.06 (dd, J=11.3/8.0 Hz, 8H, 1), 6.73 (dd, J=8.1 Hz, 8H, 2), ppm.

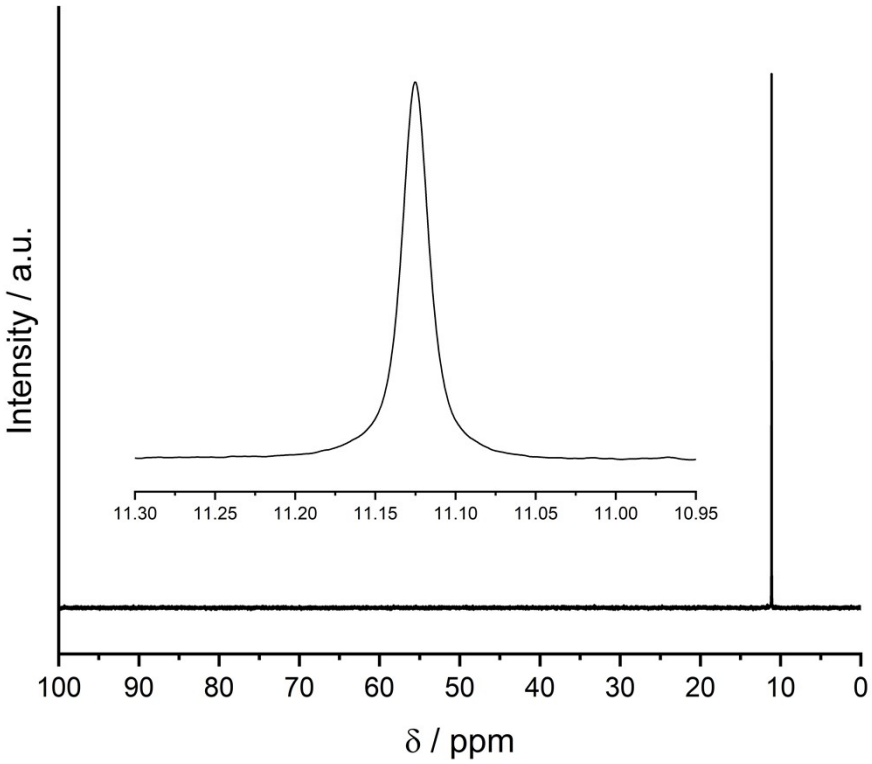

Fig. S2 ^{31}P-NMR-spectrum of 1,1,2,2-tetrakis(4-phosphonophenyl)ethylene.

^{31}P-NMR (162 MHz, 300 K, NaOD/D_2O (10 %)): δ=11.1 ppm

2 Crystal structure of the title compounds

2.1 Structure determination of the title compounds

The structures of the compound **Ga-CAU-53** was solved from PXRD data by direct space methods using FOX.[2] Indexing of the PXRD pattern gave a monoclinic cell setting (*C*2/*c*, No. 15). The structural model was completed employing force field calculations using Materials Studio[3] and finally refined with the Rietveld method[4] using the software suite Topas Academics[5]. The structure of the isostructural compounds **Al-CAU-53** and **Fe-CAU-53** were refined starting from the structural model of **Ga-CAU-53** after replacing Ga by the respective metal ion, adjusting the lattice parameter (obtained from LeBail refinements of the PXRD data) and applying force field calculations.

Compound	$[Al_2(H_2O)(H_2TPPE)] \cdot 6\ H_2O$ **Al-CAU-53**	$[Ga_2(H_2O)(H_2TPPE)] \cdot 6\ H_2O$ **Ga-CAU-53**	$[Fe_2(H_2O)(H_2TPPE)] \cdot 2\ H_2O$ **Fe-CAU-53**
Crystal system	monoclinic	monoclinic	monoclinic
SG	*C*2/*c*	*C*2/*c*	*C*2/*c*
***a* / Å**	23.960(2)	23.8290(18)	22.550(2)
***b* / Å**	5.0811(4)	5.1010(3)	5.2256(6)
***c* / Å**	27.877(4)	27.997(2)	29.039(7)
***β* / °**	77.430(7)	77.264(6)	78.153(7)
V / Å^3	3312.5(6)	3319.4(4)	3349.0(9)
R_{wp} / %	5.00	6.99	2.76
R_{Bragg}	2.08	2.74	0.84
Gof	1.33	1.24	8.31

Tab. S1 Crystallographic data of the title compounds obtained from Rietveld-refinements.

2.2 Crystal structure of Al-CAU-53 ($[Al_2(H_2O)_2(C_{26}H_{16}P_4O_{12}H_2)] \cdot xH_2O$)

The asymmetric unit of **Al-CAU-53** consists of half H_2TPPE^{4-}-molecule, one Al^{3+} ion on a general position as well as one coordinating water molecule. Additionally, there are three water molecules located in the pores. Each metal ion is octahedral surrounded by five oxygen atoms originating from five different linker molecules. The sixth oxygen is a coordinating water molecule. Each linker is connecting ten Al^{3+} ions. The interconnection by the phosphonate groups can be described using the Harris notation[6] as [2.110] for P11 and [3.111] for P21 respectively. Therefore, for each linker molecule there are two non-coordinating phosphonate-oxygen atoms, which are probably protonated. Due to the structure refinement against PXRD data the H-atom could not be located from the difference Fourier map.

The inorganic building unit is formed by the interconnection of AlO_6-octahedra and CPO_3-tetrahedra along the *b*-axis. The linker connects the inorganic rods along the *a*- and the *c*-axis thus forming a 3D-network which can be described as I^1O^2 following the classification by Cheetham.[7] Two types of pores can be distinguished in the network. The larger pores can be found between to linker molecules along the *a*-axis. The channel-type pores hold adsorbed water molecules. The smaller pores are located between two sets of the inorganic IBUs and contain only one water molecules per unit asymmetric unit.

The observed bond lengths are listed in Tab.S2

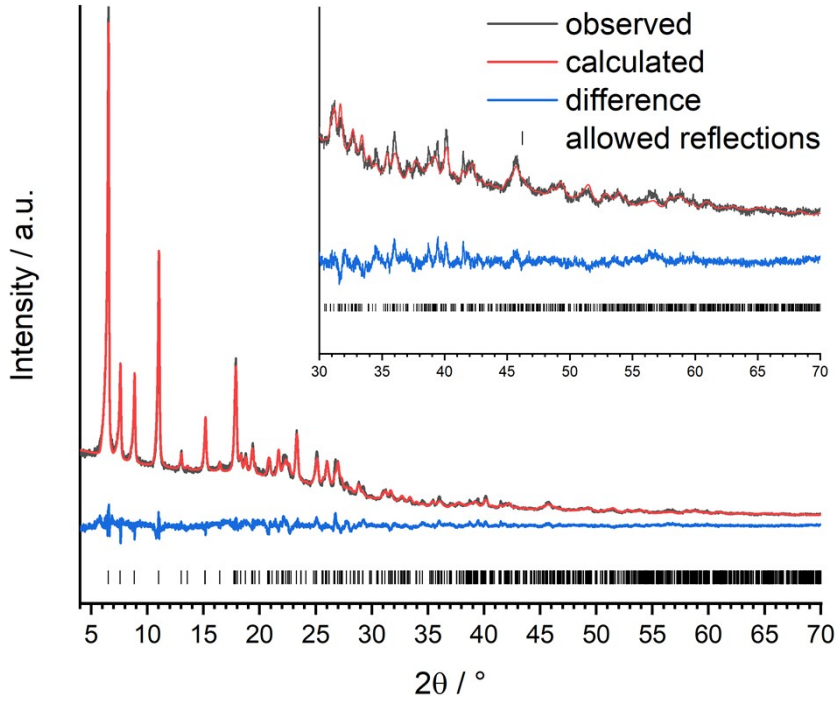

Fig. S3 Final Rietveld plot of the structure refinement of **Al-CAU-53**. The measured powder diffractogram (black line), the calculated diffractogram (red), the resulting difference (blue) and the allowed reflections (black ticks) are shown.

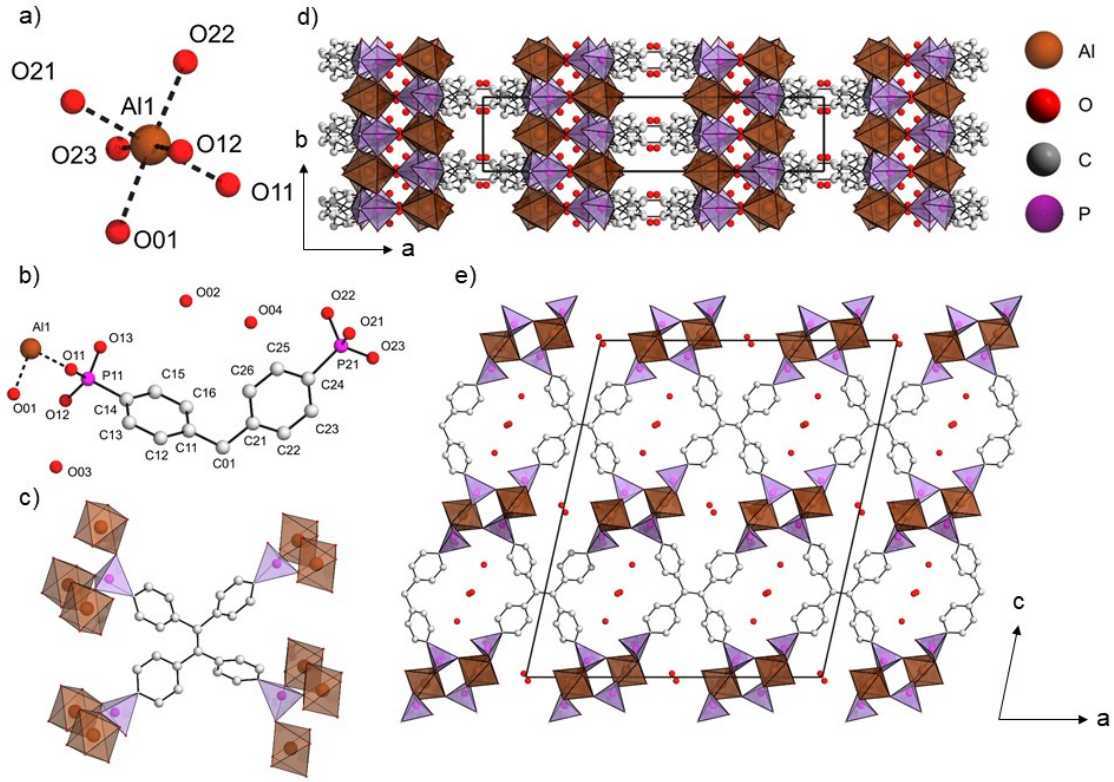

Fig. S4 a) Octahedral coordination environment of Al^{3+} ions, b) asymmetric unit of the structure of **Al-CAU-53**, c) connection of Al^{3+} ions by a linker molecule, d) representation of the structure along the *c*-axis, e) representation of the structure along the *b*-axis.

Tab. S2 Observed bond lengths in the crystal structure of **Al-CAU-53**.

Atoms	Distance / Å	Atoms	Distance / Å
Al-O01	1.94(4)	Al-O21	1.88(6)
Al-O11	1.87(5)	Al-O22	1.94(5)
Al-O12	1.90(5)	Al-O23	1.88(6)
P11-O11	1.58(5)	P21-O21	1.54(6)
P11-O12	1.53(5)	P21-O22	1.57(5)
P11-O13	1.53(5)	P21-O23	1.54(6)
P11-C14	1.79(3)	P21-C24	1.84(2)
C01-C11	1.509(9)	C01-C21	1.510(10)
C11-C12	1.394(16)	C21-C22	1.392(18)
C12-C13	1.395(17)	C22-C23	1.393(17)
C13-C14	1.392(16)	C23-C24	1.39(2)
C14-C15	1.396(17)	C24-C25	1.40(2)
C15-C16	1.391(16)	C25-C26	1.394(14)
C16-C11	1.394(16)	C26-C21	1.395(18)
C01-C01	1.358(5)		

2.3 Crystal structure of Ga-CAU-53 ($[Ga_2(H_2O)_2(C_{26}H_{16}P_4O_{12}H_2)] \cdot xH_2O$)

The crystal structure of the compound $[Ga_2(H_2O)_2(C_{26}H_{16}P_4O_{12}H_2)]$ is isostructural to the discussed structure of $[Al_2(H_2O)_2(C_{26}H_{16}P_4O_{12}H_2)]$. Caused by the bigger ionic radius of Ga^{3+} compared to Al^{3+} the M-O bond lengths are slightly longer in the structure of $[Ga_2(H_2O)_2(C_{26}H_{16}P_4O_{12}H_2)]$ and meet the expectations as well as the covalent bond lengths do (Tab. S3). Only the orientation of the first CPO_3-group (C14-P11-O11-O12-O13, [2.110]) differs. The non-coordinating Oxygen O13 is pointing towards the smaller cavities in contrast to the orientation towards the bigger cavities in $[Al_2(H_2O)_2(C_{26}H_{16}P_4O_{12}H_2)]$ (Fig. 3 in the manuscript).

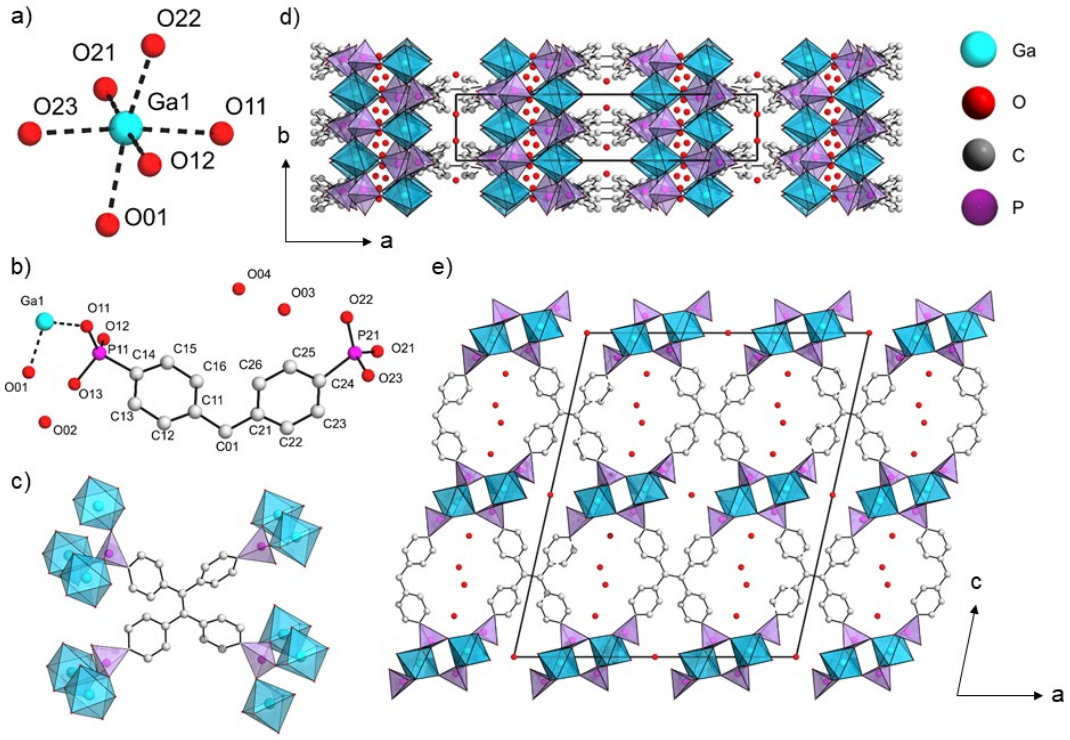

Fig. S5 Octahedral coordination environment of Ga^{3+} ions, b) asymmetric unit of the structure of **Ga-CAU-53**, c) connection of Ga^{3+} ions by a linker molecule, d) representation of the structure along the *c*-axis, e) representation of the structure along the *b*-axis.

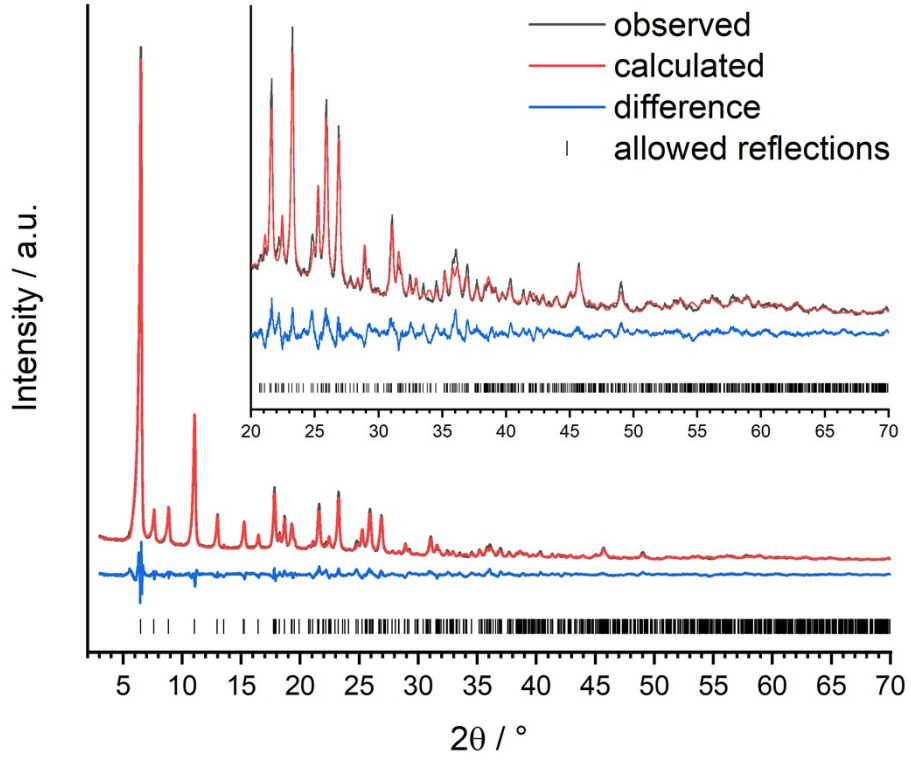

Fig. S6 Final Rietveld plot of the structural refinement of **Ga-CAU-53**. The measured powder diffractogram (black line), the calculated diffractogram (red), the resulting difference (blue) and the allowed reflections (black ticks) are shown.

Tab. S3 Bond lengths in Observed bond lengths in the crystal structure of **Ga-CAU-53**.

Atoms	Distance / Å	Atoms	Distance / Å
Ga-O01	2.09(3)	Ga-O21	1.93(5)
Ga-O11	2.02(4)	Ga-O22	1.92(4)
Ga-O12	2.04(5)	Ga-O23	2.06(3)
P11-O11	1.55(5)	P21-O21	1.52(6)
P11-O12	1.58(6)	P21-O22	1.50(5)
P11-O13	1.56(3)	P21-O23	1.53(6)
P11-C14	1.75(3)	P21-C24	1.77(3)
C01-C11	1.440(12)	C01-C21	1.440(11)
C11-C12	1.39(3)	C21-C22	1.39(3)
C12-C13	1.39(2)	C22-C23	1.39(2)
C13-C14	1.38(4)	C23-C24	1.39(4)
C14-C15	1.38(5)	C24-C25	1.39(5)
C15-C16	1.38(3)	C25-C26	1.38(2)
C16-C11	1.39(4)	C26-C21	1.38(4)
C01-C01	1.380(5)		

2.4 Crystal structure of Fe-CAU-53 ($[Fe_2(H_2O)(C_{26}H_{16}P_4O_{12}H_2)] \cdot xH_2O$)

The crystal structure of $[Fe_2(H_2O)(C_{26}H_{16}P_4O_{12}H_2)]$ is isostructural to the one of $[Al_2(H_2O)(C_{26}H_{16}P_4O_{12}H_2)]$. A refinement of a structural model based on **Al-CAU-53** was carried out. The final lattice parameter as well as crystallographic data is given in Tab. S1. The bond lengths are shown in Tab. S4. The relatively high standard deviations on certain bond lengths are due to an inferior quality of the obtained PXRD data.

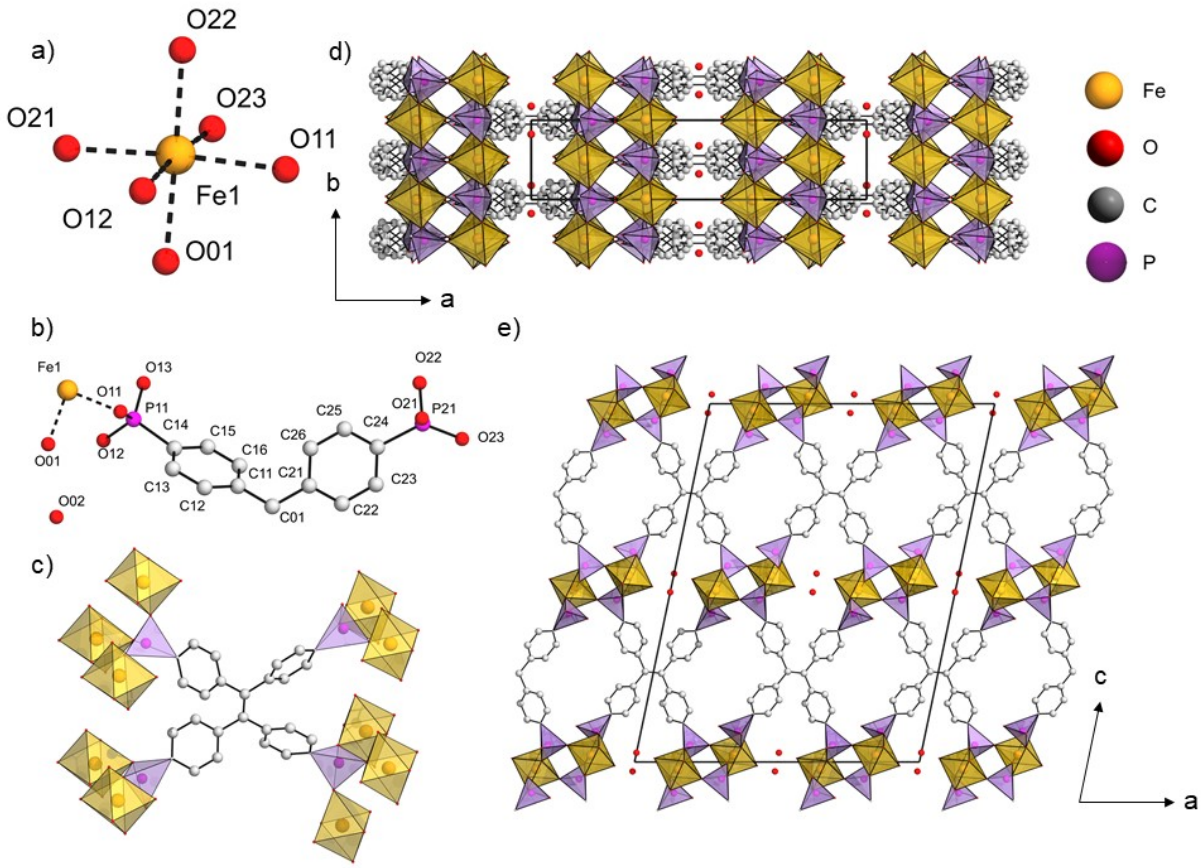

Fig. S7 Octahedral coordination environment of Fe^{3+} ions, b) asymmetric unit of the structure of **Fe-CAU-53**, c) connection of FeO_6 polyhedra by a linker molecule, d) representation of the structure along the *c*-axis, e) representation of the structure along the *b*-axis.

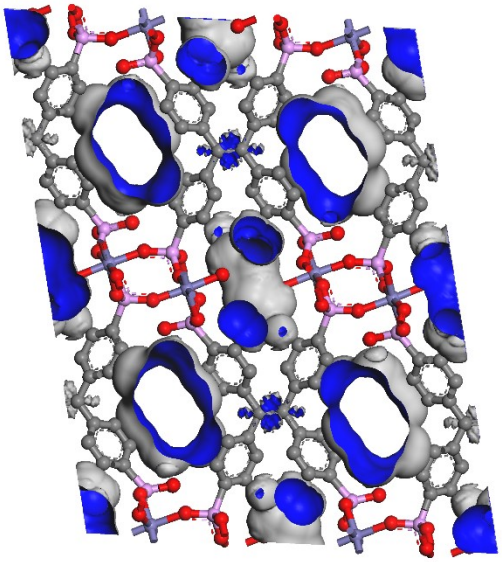

Fig. S8 Connolly surfaces calculated for **Fe-CAU-53**. For the simulation, a water molecule (diameter: 2.6 Å) was employed as a probe molecule. The calculations was accomplished using Materials Studio.[3] The small and large pores are clearly distinguishable.

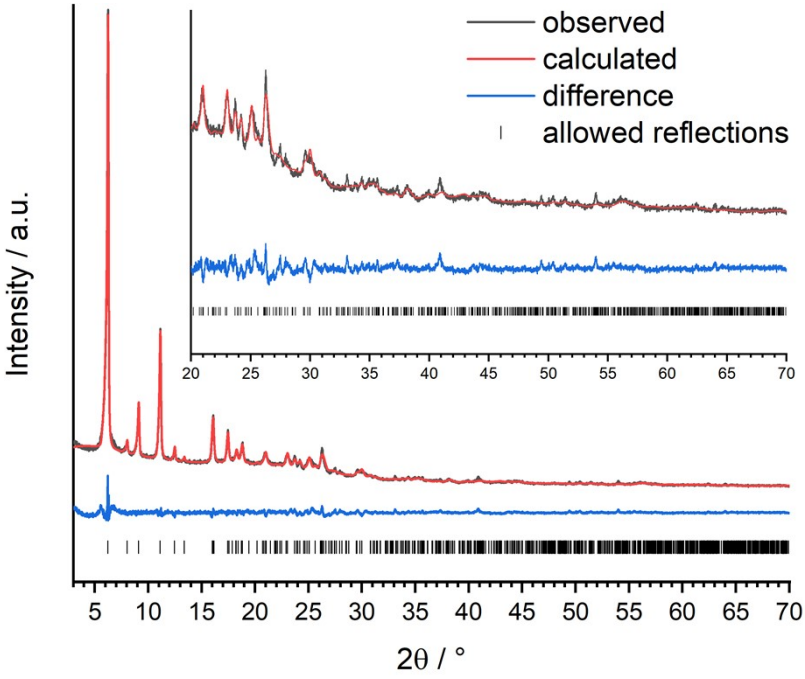

Fig. S9 Final Rietveld plot of the structural refinement of **Fe-CAU-53**. The measured powder diffractogram (black line), the calculated diffractogram (red), the resulting difference (blue) and the allowed reflections (black ticks) are shown.

Tab. S4 Bond lengths in Observed bond lengths in the crystal structure of **Fe-CAU-53**.

Atoms	Distance / Å	Atoms	Distance / Å
Fe-O01	2.09(12)	Fe-O21	2.06(10)
Fe-O11	2.09(5)	Fe-O22	2.03(11)
Fe-O12	1.99(11)	Fe-O23	2.08(11)
P11-O11	1.56(11)	P21-O21	1.55(11)
P11-O12	1.56(12)	P21-O22	1.56(12)
P11-O13	1.56(8)	P21-O23	1.54(10)
P11-C14	1.88(5)	P21-C24	1.85(4)
C01-C11	1.5101(3)	C01-C21	1.5099(3)
C11-C12	1.3951(2)	C21-C22	1.3949(2)
C12-C13	1.3948(2)	C22-C23	1.3949(3)
C13-C14	1.3950(1)	C23-C24	1.3949(1)
C14-C15	1.3949(2)	C24-C25	1.3950(2)
C15-C16	1.3952(2)	C25-C26	1.3949(3)
C16-C11	1.3950(1)	C26-C21	1.3951(1)
C01-C01	1.2980(1)		

2.5 Topological analyses of the CAU-53 network

All topological analyses were carried out using ToposPro[8], Systre and 3dt.[9] A standard simplification method as implemented in ToposPro was applied to obtain the underlying network in the CAU-53 structures. Following this method, the linker molecules in the structure can be described as 10-connected nodes, while the metal-centres can be simplified to 5-c nodes. Originally, a third node (1-c) originating from the coordinated water molecule was identified, but later deleted after a careful investigation in order to preserve a net. The remaining network topology was identified as **fit**. Figure S.10 shows the network obtained with the standard simplification method (left) as seen along (010) and the tiling in the high-symmetry form (*I*4/*mmm*) of the 5,10-c **fit** net (right). This topological network differs from the ones described before employing the same linker molecule. However, a **fit** net was reported for a coordination polymer utilizing a tetraphosphonic acid.[10]

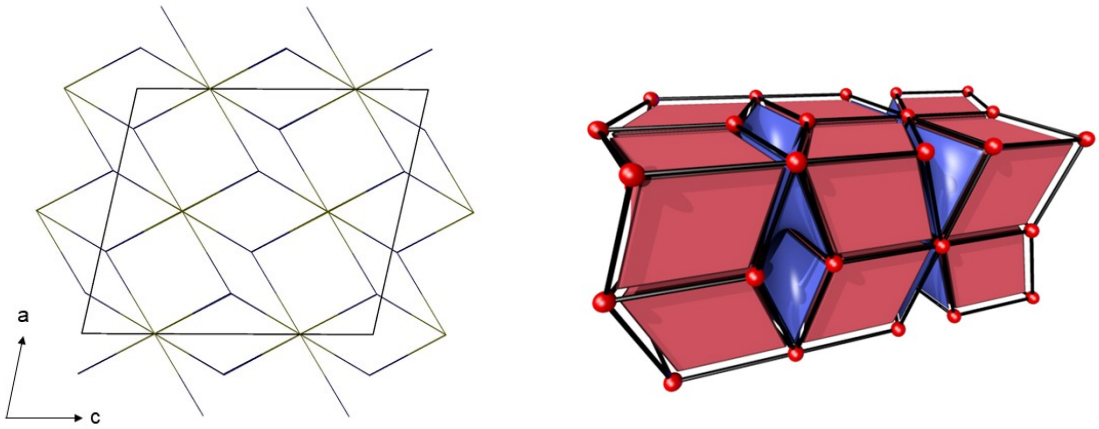

Fig. S10 Left: Simplified network obtained employing the standard simplification method and the **CAU-53** structure resulting in the binodal 5,10-c net **fit**. Right: Tiling of the high-symmetry form of the simplified net visualised with 3dt as part of the Gavrog package.

3 Thermal properties and thermogravimetric measurements

The thermal properties of the three title compounds were studied by temperature dependent powder X-ray diffraction. All three compounds were placed in 0.5 mm quartz capillaries and studied between 30 °C and their decomposition temperature. Samples were heated in steps of 10 or 20 °C while PXRD data was collected.

Datasets from thermogravimetric measurements were collected for the title compounds respectively. All TG-plots (Fig. S13, S15 and S18) show a mass loss around 100 °C that is attributed to the loss of adsorbed water molecules. A second significant mass loss is assigned to the combustion of the linker-molecules and the formation of different metal phosphates. In all cases, this combustion is not completely achieved at 800 °C, so the residues were not further investigated.

3.1 VT-PXRD- and TG-data for Al-CAU-53

Figure 5 in the manuscript shows the results from the VT-PXRD experiment as a 2D contour plot. In the temperature range of 30 – 330 ° C, no significant structural changes in **Al-CAU-53** are observed. Therefore, the data is suitable for a sequential refinement of the lattice parameters in order to evaluate small changes of the unit cell parameters.

The change of the lattice parameters *a*, *b* and *c* in the structure of Al-CAU-53 were analyzed with a sequential refinement using the Rietveld algorithm as implemented in TOPAS Academics [5]. For the studies only the lattice parameters *a*, *b*, *c* and *β* as well as one temperature factor for all atoms and the occupancies of the guest molecules were refined (besides basic parameters such as background or peak shape). Figure S11 shows the evolution of the *a*-, *b*- and *c*-lattice parameter in the structure of **Al-CAU-53** while Table S5 contains the numerical data.

The R_{wp} of the refinements was used to determine the quality of the results. As can be seen in Figure S12, there is an increase of the R_{wp} at temperatures higher than 330 °C, which indicates significant structural changes that could not be evaluated based on the obtained PXRD data. For the evolution of the lattice parameters, only the results at temperatures lower than 350 °C were used.

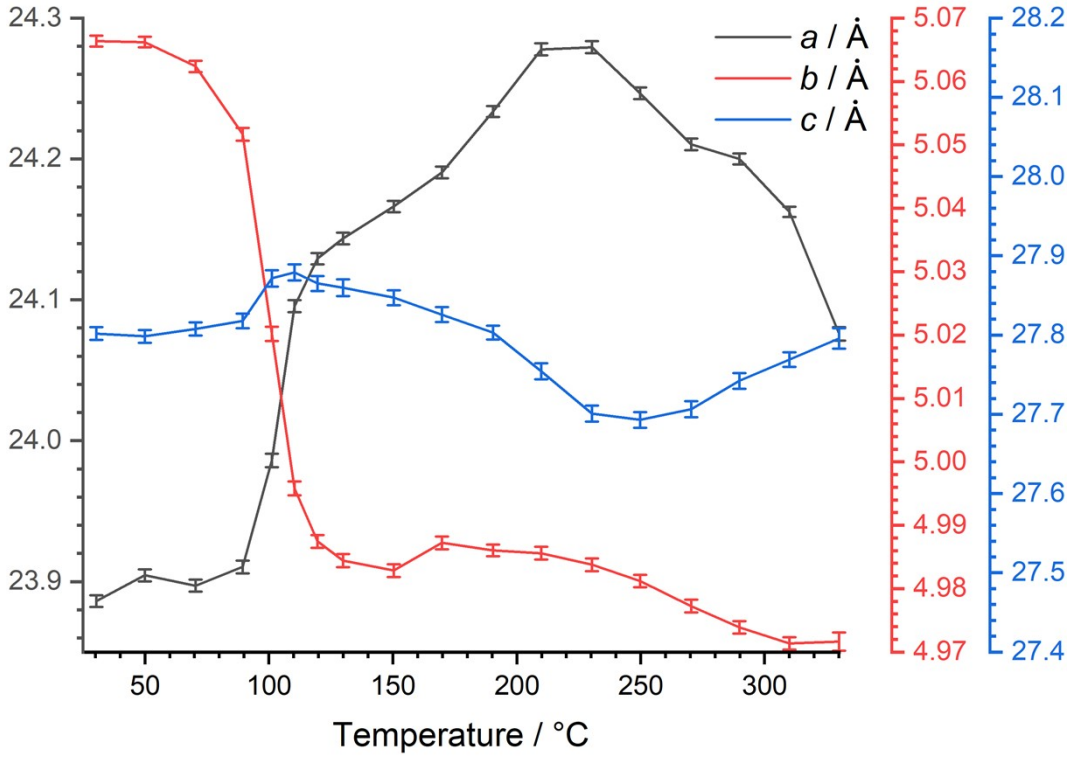

Fig. S11 Evolution of the lattice parameters in the structure of **Al-CAU-53** during the VT-PXRD measurement obtained from a sequential Rietveld refinement of the lattice parameters.

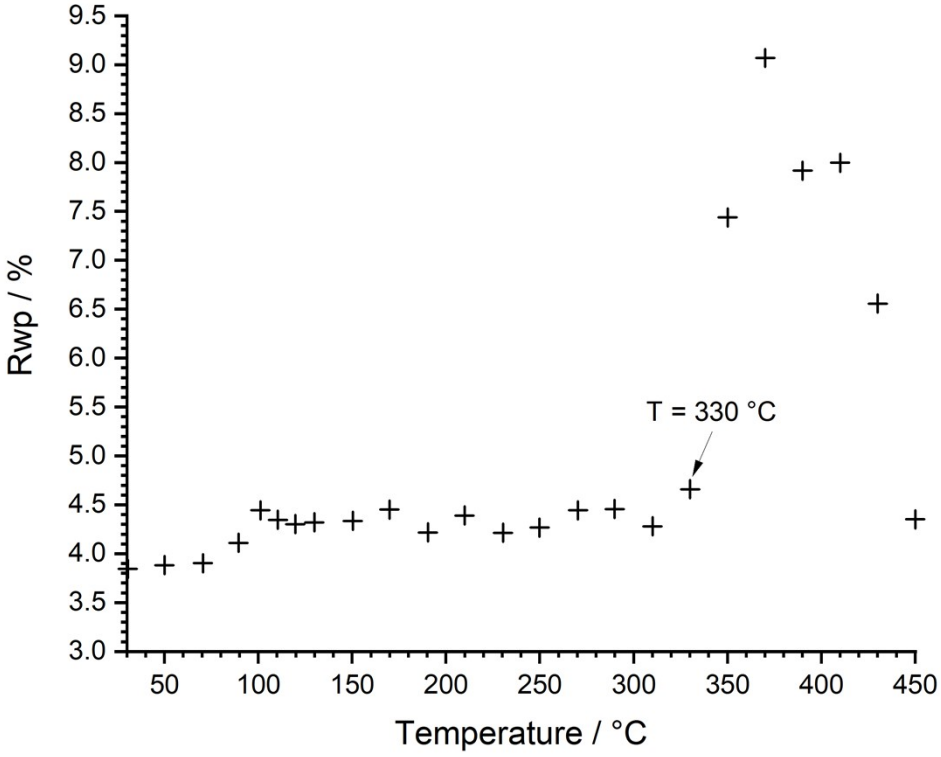

Fig. S12 Evolution of the R_{wp}-value from the sequential Rietveld-refinement of the lattice parameters and temperature factors in the structure of **Al-CAU-53** based on the VT-PXRD-data.

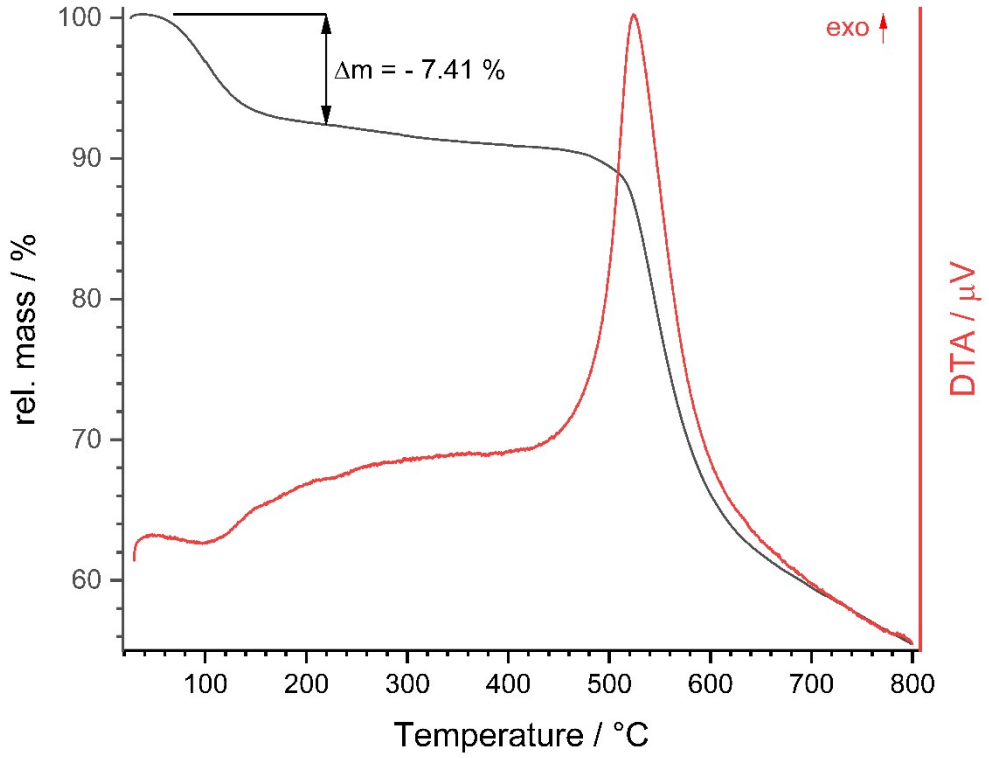

Fig. S13 TG- and DTA-plot from the thermogravimetric measurement of **Al-CAU-53**. The first mass loss can be attributed to the loss of three water molecules per sum formula.

Table S5 Results from the sequential Rietveld-refinement of the lattice parameters and temperature factors in the structure of **Al-CAU-53** based on the VT-PXRD-data.

Temperature / °C	R_{wp} / %	*a* / Å	*b* / Å	*c* / Å	*β* / Å	Unit cell vol. / Å^3
30.4	3.84	23.886(4)	5.0664(9)	27.802(8)	77.471(11)	3284.4(13)
49.9	3.88	23.904(4)	5.0662(9)	27.798(8)	77.47(11)	3286.4(13)
70.4	3.90	23.897(4)	5.0624(9)	27.808(8)	77.494(11)	3284.2(13)
89.4	4.11	23.91(5)	5.0517(10)	27.818(9)	77.565(11)	3281.2(14)
101.1	4.44	23.986(5)	5.0202(11)	27.871(10)	77.78(12)	3280.1(16)
110.3	4.35	24.095(4)	4.9958(11)	27.879(10)	77.913(10)	3281.6(15)
119.6	4.30	24.129(4)	4.9875(10)	27.865(9)	78.001(9)	3280.1(14)
129.8	4.32	24.144(4)	4.9844(11)	27.86(10)	78.025(9)	3279.8(15)
150.3	4.33	24.166(4)	4.9829(10)	27.847(9)	78.03(9)	3280.4(14)
169.8	4.45	24.19(4)	4.9872(10)	27.826(9)	78.039(10)	3284.1(14)
190.3	4.22	24.234(4)	4.986(9)	27.803(9)	78.038(9)	3286.5(13)
209.8	4.39	24.278(4)	4.9856(10)	27.754(10)	78.05(10)	3286.6(15)
230.3	4.21	24.279(4)	4.9838(10)	27.701(10)	78.082(10)	3279.6(15)
249.8	4.27	24.247(4)	4.9812(10)	27.693(10)	78.083(9)	3272.6(15)
270.3	4.44	24.21(4)	4.9773(10)	27.707(10)	78.08(9)	3266.7(15)
289.8	4.46	24.2(4)	4.9739(10)	27.742(10)	78.076(9)	3267.2(14)
310	4.28	24.163(4)	4.9714(10)	27.769(10)	78.079(8)	3263.7(13)
330	4.66	24.076(5)	4.9716(14)	27.796(13)	78.137(10)	3256(19)
350	7.44	23.21(4)	4.948(11)	26.8(7)	78.46(7)	3015(11)
370	9.07	22.86(5)	4.946(14)	26.79(9)	78.03(10)	2963(14)
390	7.92	21.64(4)	5.011(14)	27.28(9)	79.45(9)	2909(14)
410	8.00	21.49(5)	5.012(14)	27.47(11)	79.25(11)	2906(16)
430	6.56	20.84(7)	4.994(19)	27.82(11)	78.54(13)	2837(18)
450	4.35	20.1(2)	4.98(4)	28(3)	78.02(15)	2750(50)

3.2 Thermogravimetric data for Ga-CAU-53

The VT-PXRD-data for **Ga-CAU-53** is discussed in the manuscript and shown in Figure 5. The TG-plot is shown in Figure S14.

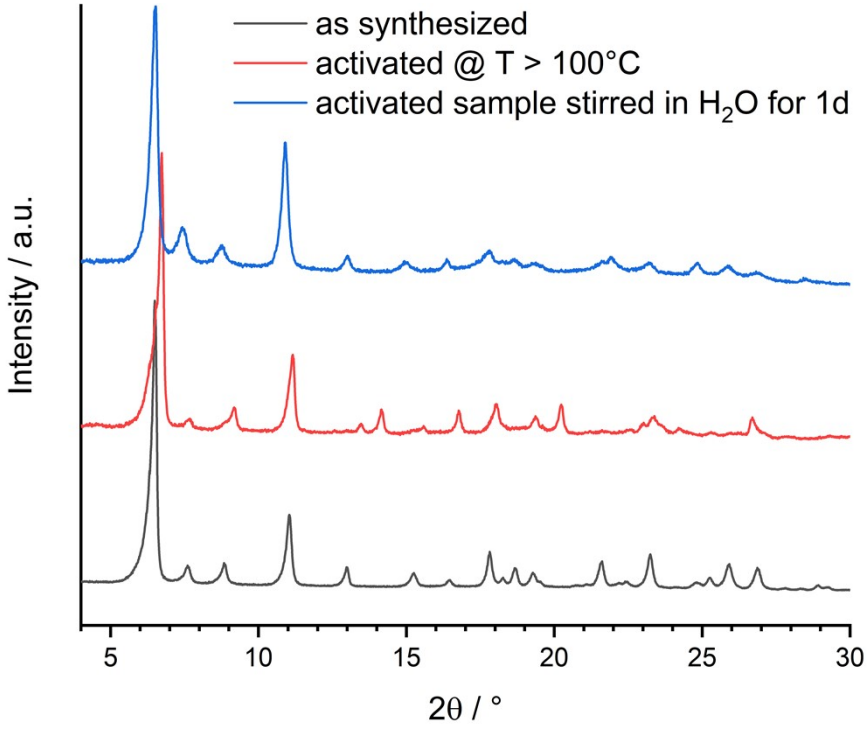

Fig. S14 Comparison of PXRD patterns of **Ga-CAU-53** as synthesized (black), activated at 100 °C (red) and after stirring the activated sample in water for one day (blue).

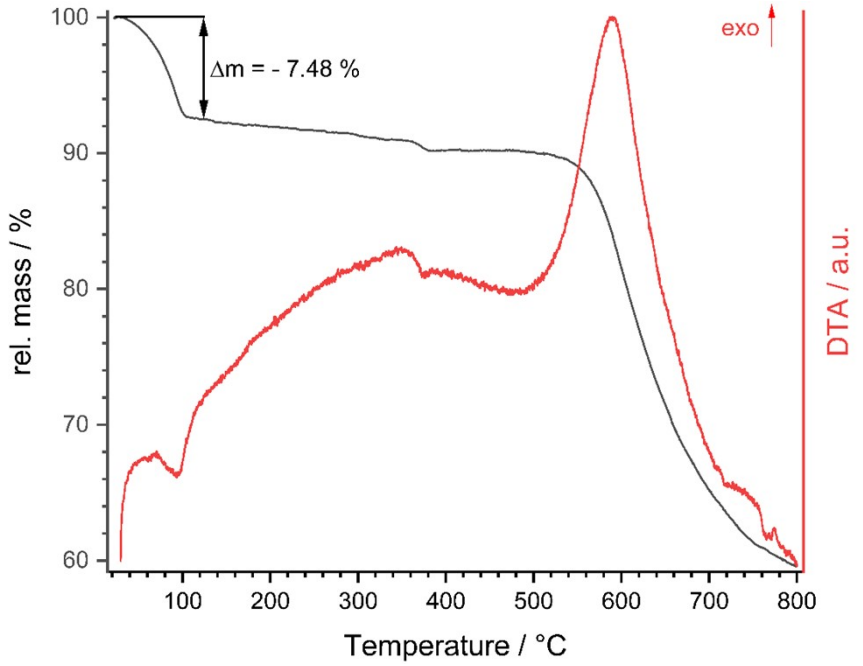

Fig. S15 TG- and DTA-plot of **Ga-CAU-53**. The first mass loss can be attributed to the loss of 3.5 water molecules per sum formula.

3.3 VT-PXRD- and TG-data for Fe-CAU-53

The thermal properties of **Fe-CAU-53** are discussed in the main manuscript. Figure S16 shows the data from the VT-PXRD experiment and Figure S18 shows the data obtained from thermogravimetric investigations.

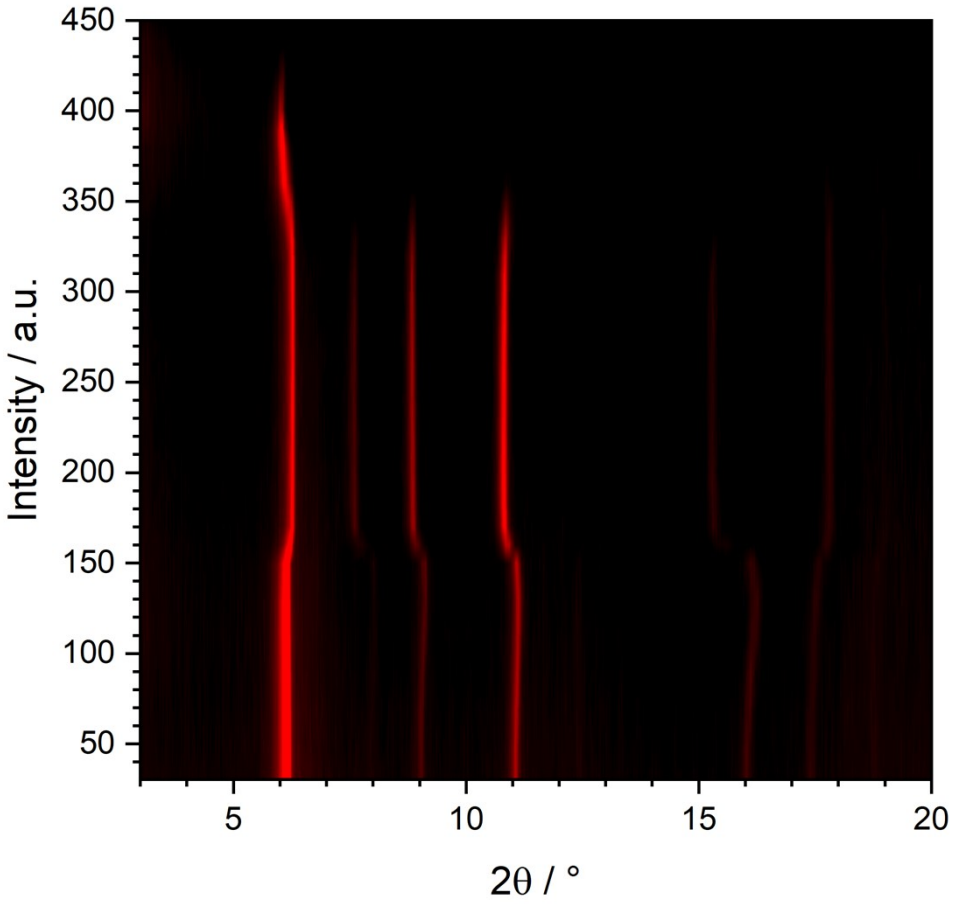

Fig. S16 Variable temperature powder X-ray diffraction data of **Fe-CAU-53**. For the measurement, the sample was placed in a 0.5 mm quartz capillary and heated in steps of 10 °C.

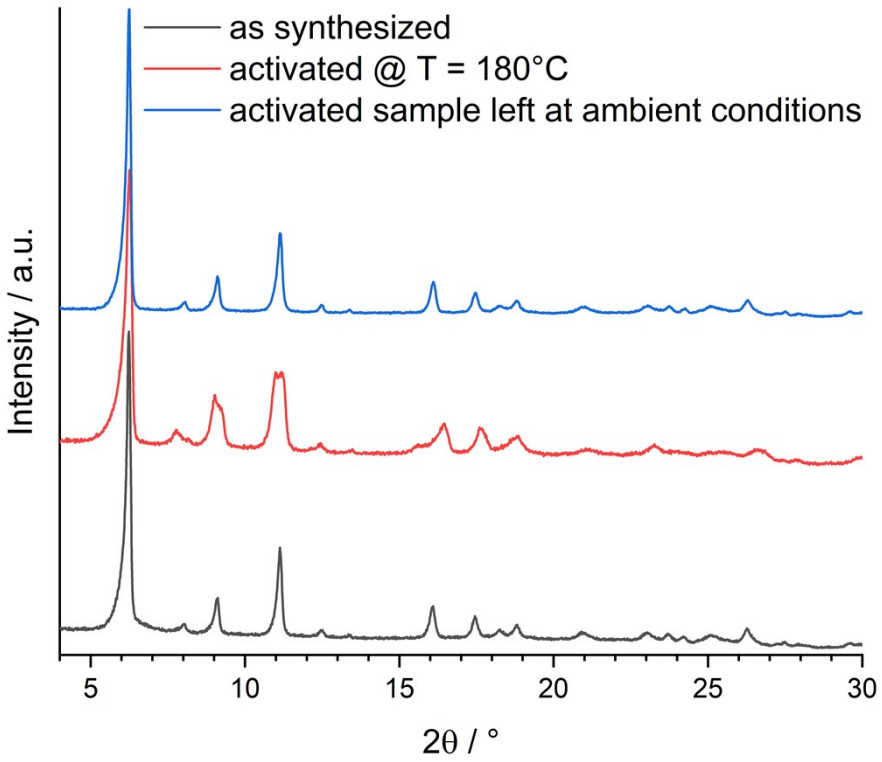

Fig. S17 Comparison of PXRD patterns of **Fe-CAU-53** as synthesized (black), activated at 180 °C (red) and leaving the sample at ambient conditions for three days (blue).

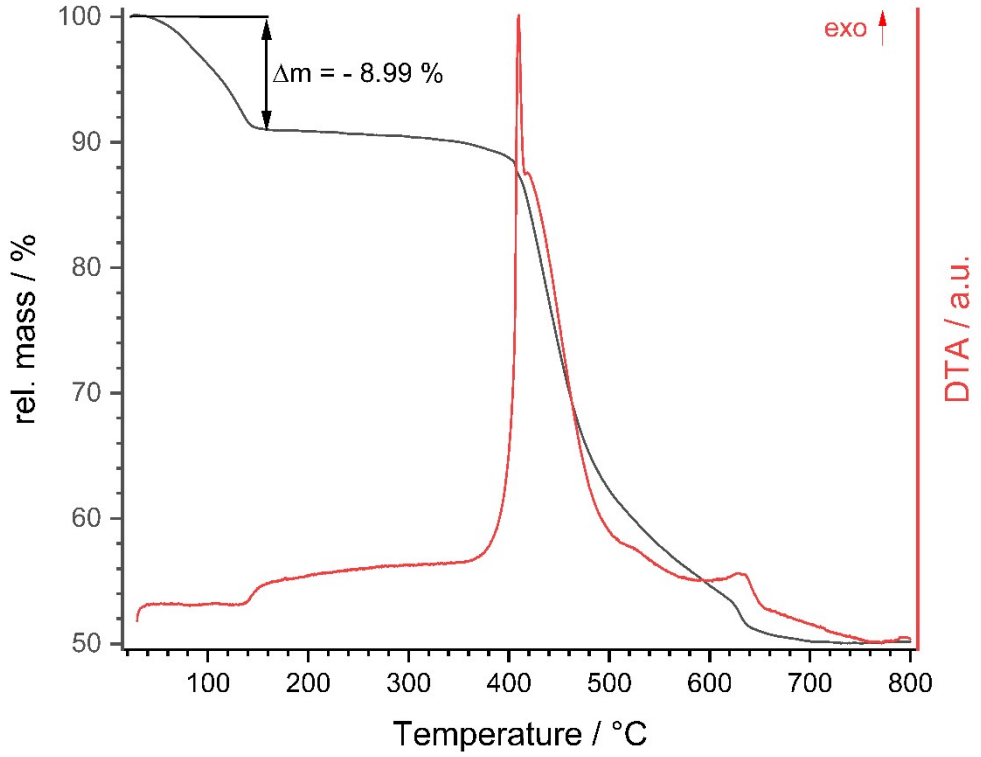

Fig. S18 TG- and DTA-plot of **Fe-CAU-53**. The first mass loss can be attributed to the loss of four water molecules per sum formula.

4 N_2- and H_2O-sorption properties

Nitrogen and water ad- and desorption isotherms were collected for the title compounds. Before the measurements, the samples were activated at reduced pressure at 180 °C (N_2-ad-/desorption) and 150 °C (H_2O-ad-/desorption) for 16 hours.

4.1 N_2- and H_2O-sorption behaviour of Al-CAU-53

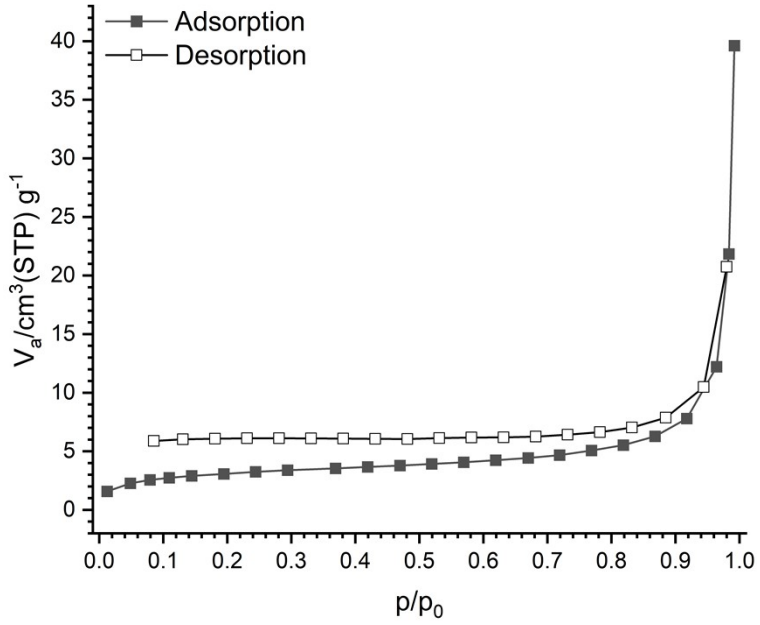

Fig. S19 N_2-adsorption (filled squares) and desorption (unfilled squares) isotherms measured for samples of **Al-CAU-53**.

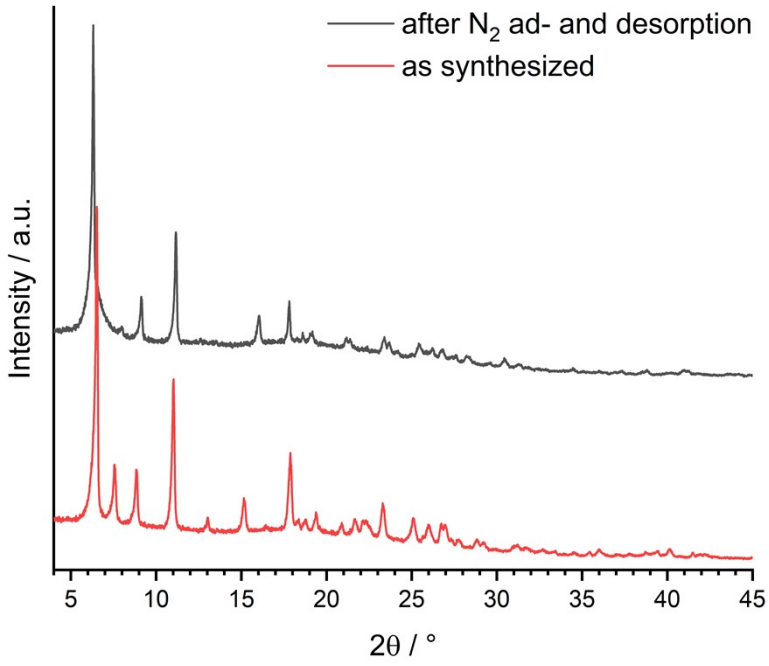

Fig. S20 PXRD-pattern of **Al-CAU-53** after N_2 ad- and desorption experiments. For the activation of the sample, a temperature of 180 °C was applied for 16 hours.

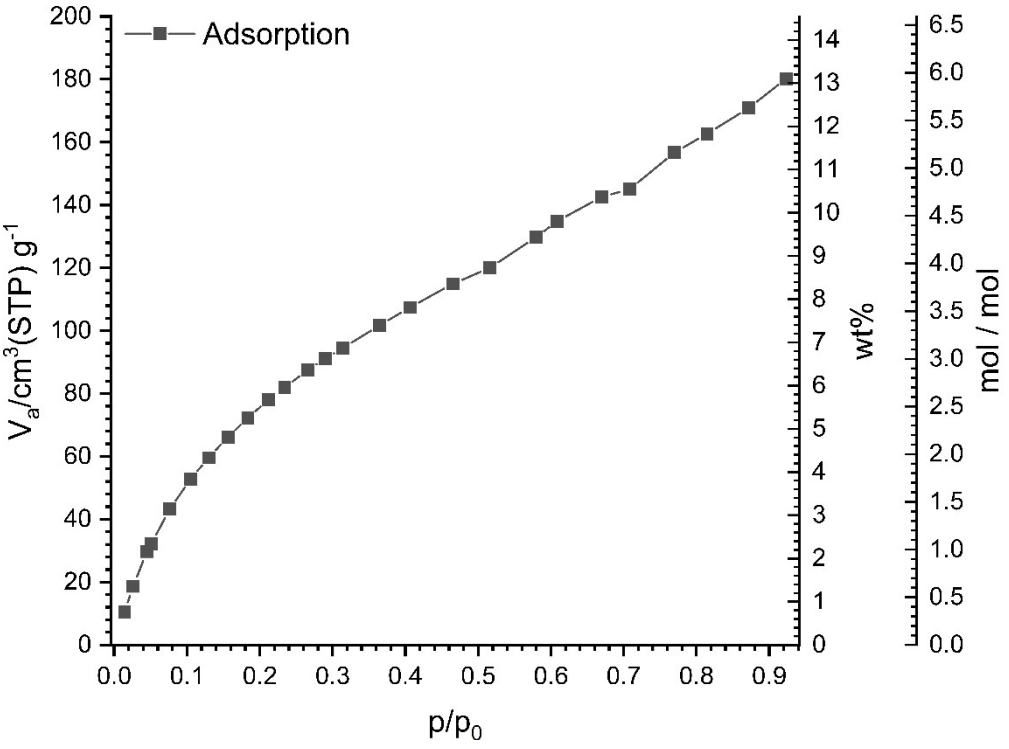

Fig. S21 Water adsorption (filled squares) and desorption (unfilled squares) isotherms measured for samples of **Al-CAU-53**. For the activation of the sample, a temperature of 150 °C was applied for 16 hours.

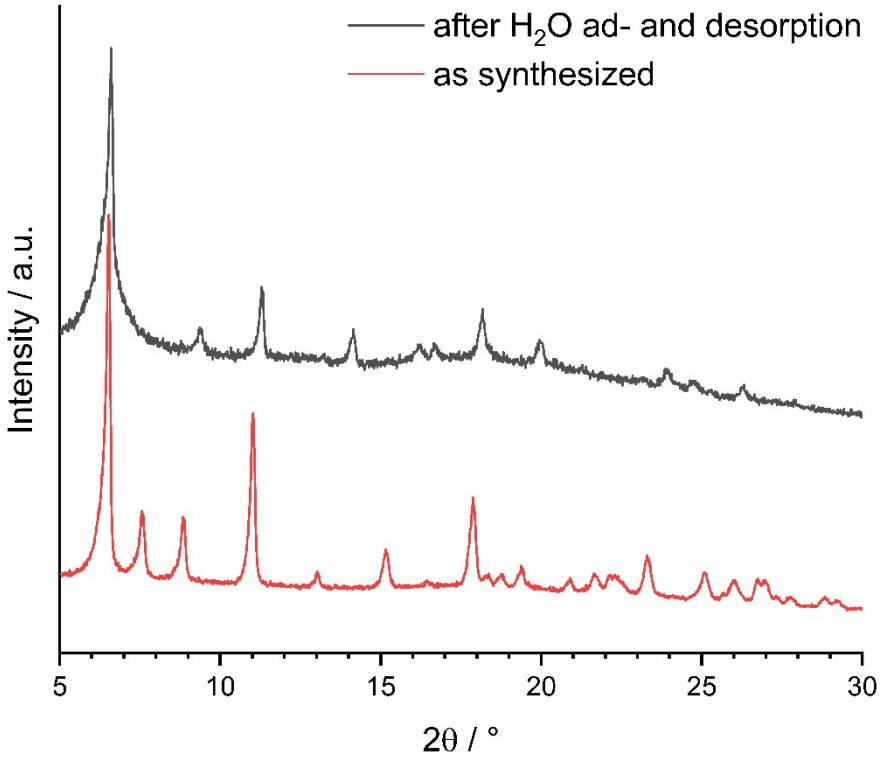

Fig. S22 PXRD-pattern of **Al-CAU-53** after H_2O-ad- and desorption experiments.

4.2 N_2- and H_2O-sorption behaviour of Ga-CAU-53

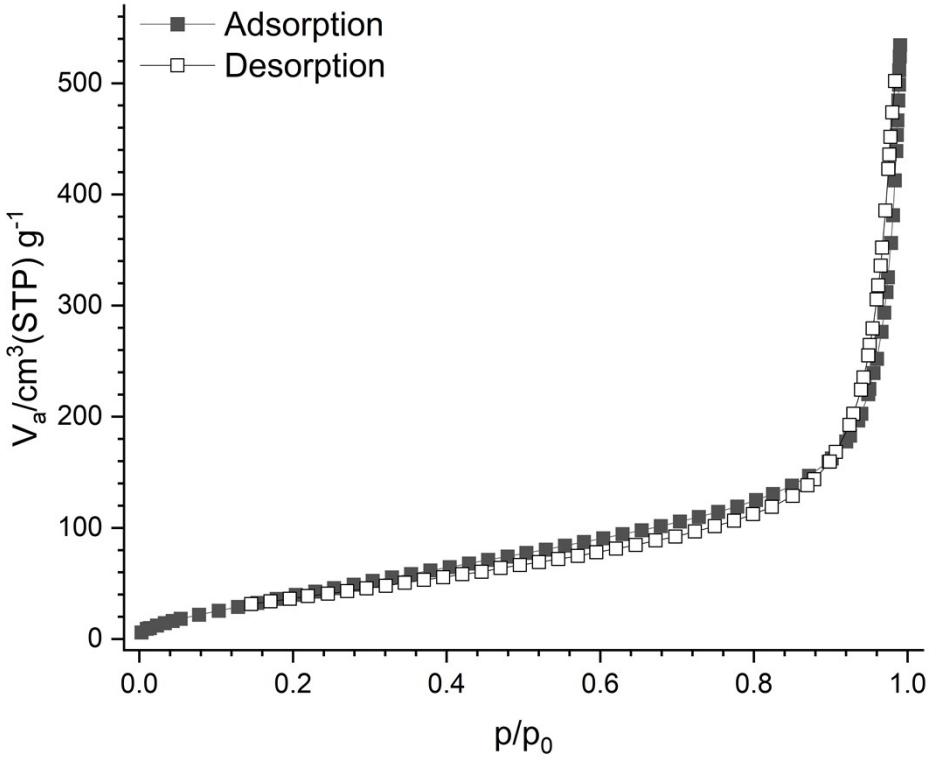

Fig. S23 N_2-adsorption (filled squares) and desorption (unfilled squares) isotherms measured for samples of **Ga-CAU-53**.

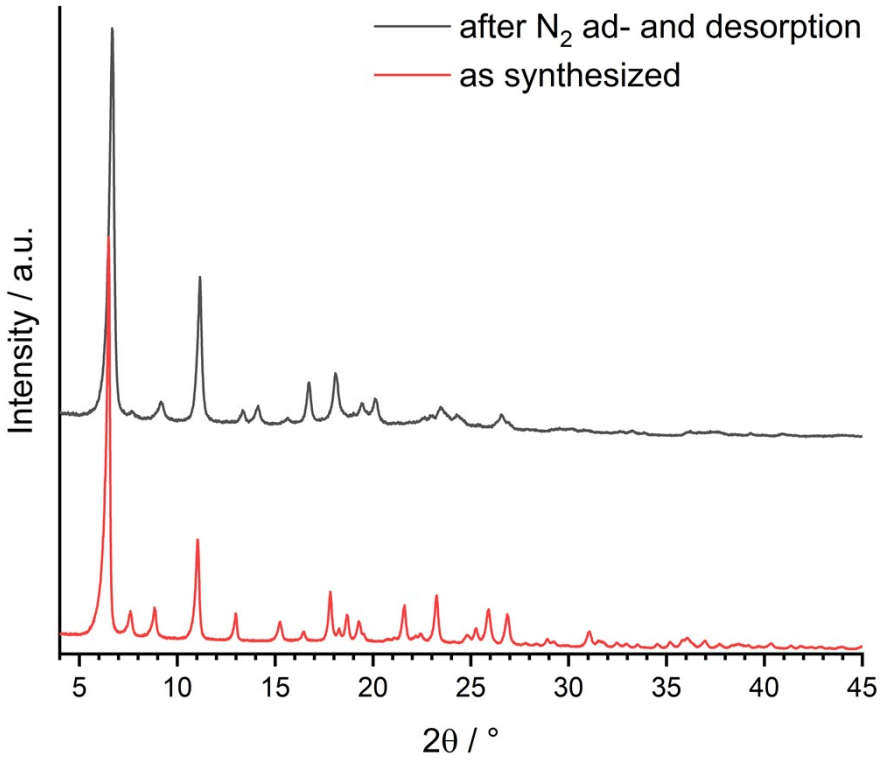

Fig. S24 PXRD-pattern of **Ga-CAU-53** after N_2 ad- and desorption experiments. For the activation of the sample, a temperature of 180 °C was applied for 16 hours.

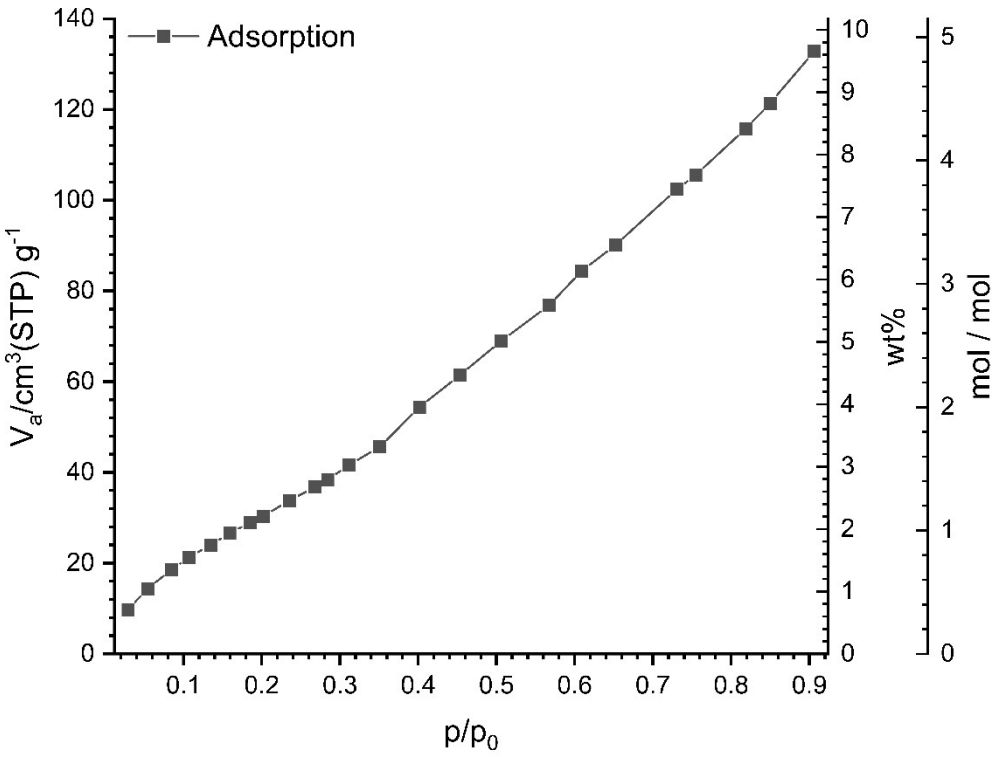

Fig. S25 Water adsorption (filled squares) and desorption (unfilled squares) isotherms measured for samples of **Ga-CAU-53**. For the activation of the sample, a temperature of 150 °C was applied for 16 hours.

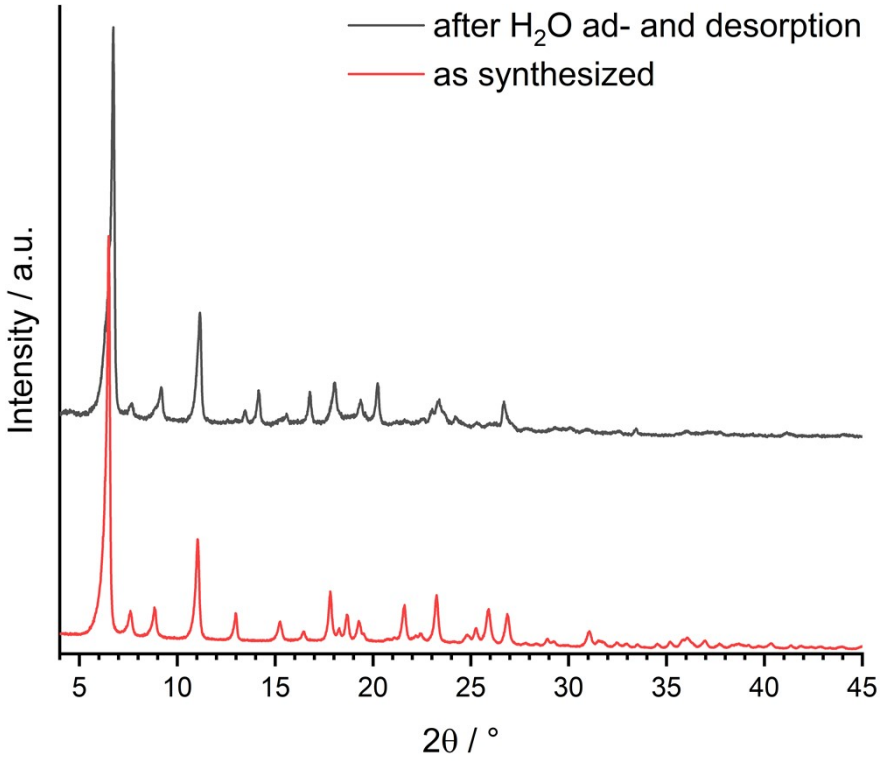

Fig. S26 PXRD-pattern of **Ga-CAU-53** after H_2O ad- and desorption experiments. For the activation of the sample, a temperature of 150 °C was applied for 16 hours.

4.3 N_2- and H_2O-sorption behaviour of Fe-CAU-53

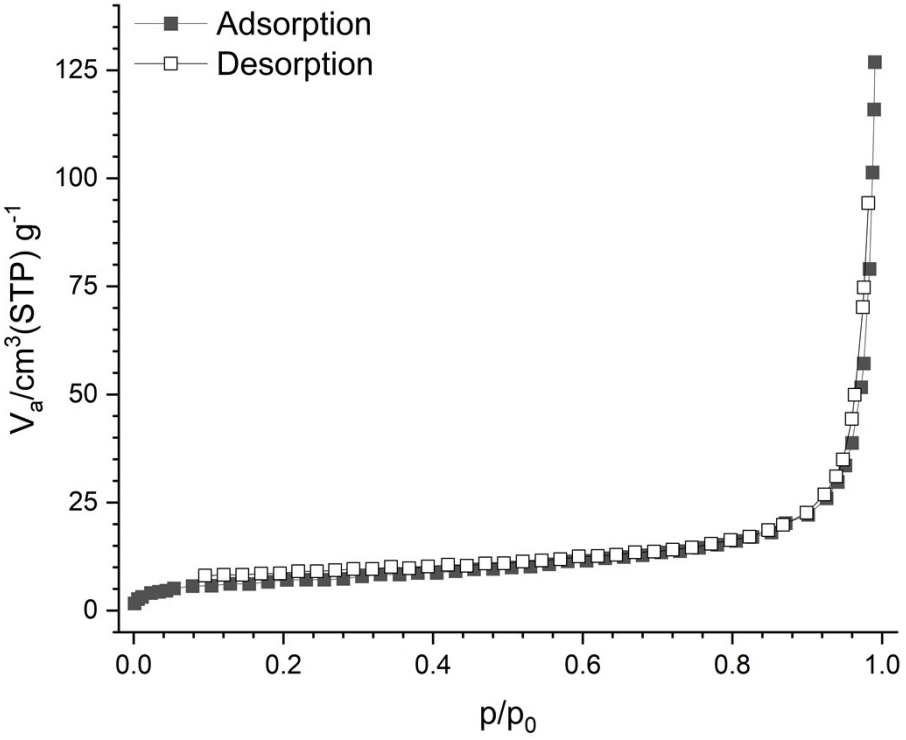

Fig. S27 N_2-adsorption (filled squares) and desorption (unfilled squares) isotherms measured for a sample of **Fe-CAU-53**.

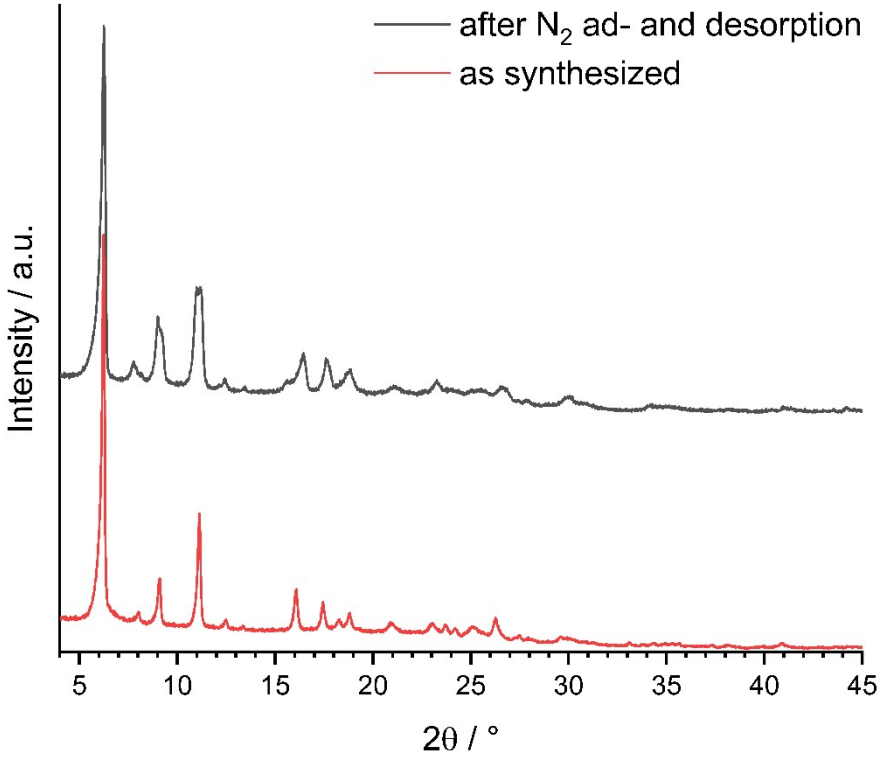

Fig. S28 PXRD-pattern of **Fe-CAU-53** after N_2 ad- and desorption experiments. For the activation of the sample, a temperature of 180 °C was applied for 16 hours.

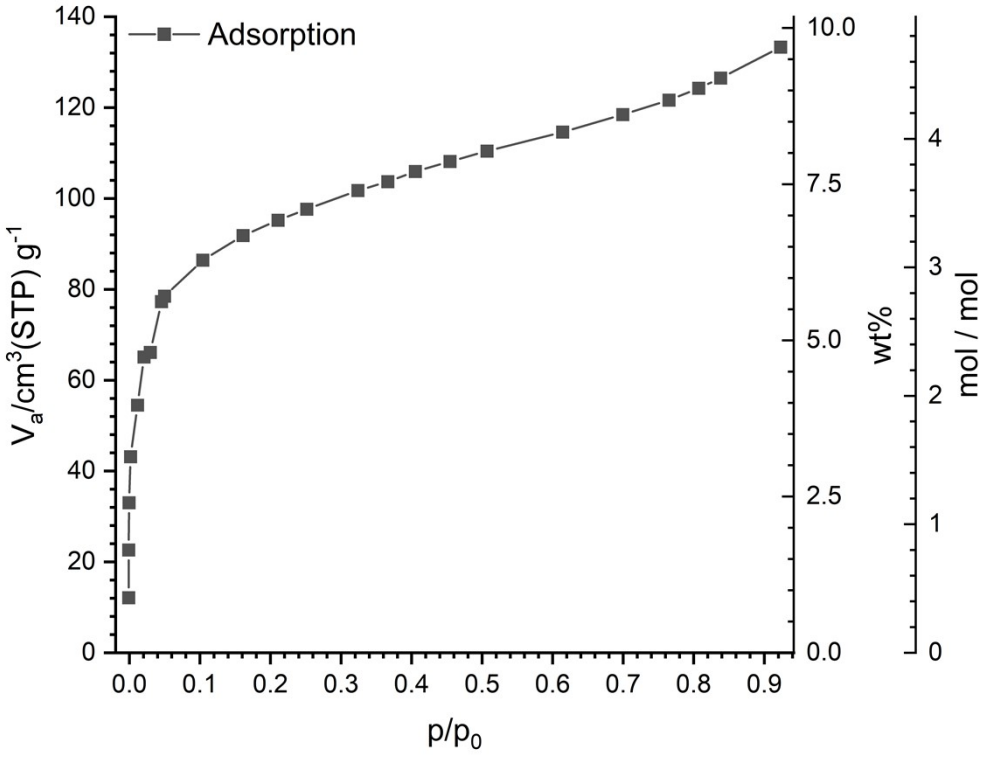

Fig. S29 Water adsorption (filled squares) and desorption (unfilled squares) isotherms measured for samples of **Fe-CAU-53**. For the activation of the sample, a temperature of 150 °C was applied for 16 hours.

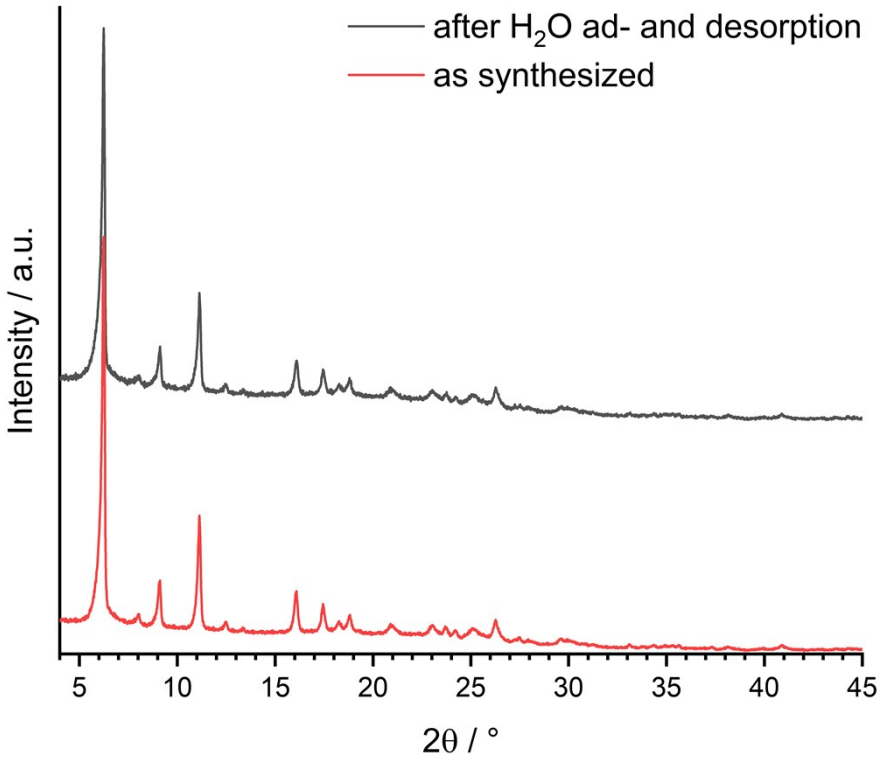

Fig. S30 PXRD-pattern of **Fe-CAU-53** after H_2O ad- and desorption experiments. For the activation of the sample, a temperature of 150 °C was applied for 16 hours.

5 MIR-spectroscopy of M-CAU-53 (M= Al, Ga, Fe)

The title compounds were characterised by IR-spectroscopy (Figs. 31-33). The assigned bands are summarized in Table S6.

Tab. S6 Assignment of observed bands in the IR-spectra of the title compounds.

IR-Band	Wavenumber / cm^{-1}	**Al-CAU-53**	**Ga-CAU-53**	**Fe-CAU-53**
OH-str.	3760-3200	3617	3611	3619
CH str.	3050	3071	3075	3062
Aromatic ring in plane str.	1600, 1500	1600, 1501	1604, 1498	1601, 1502
C=C vib.	1600-1395	1558, 1396	1556, 1396	1558, 1396
P=O str.	1250-1150	1141	1138	1141
C-PO_3 str.	1200-900	1075	1083	1077
(O=)P-O str.	1040-910	1043	1029	1036

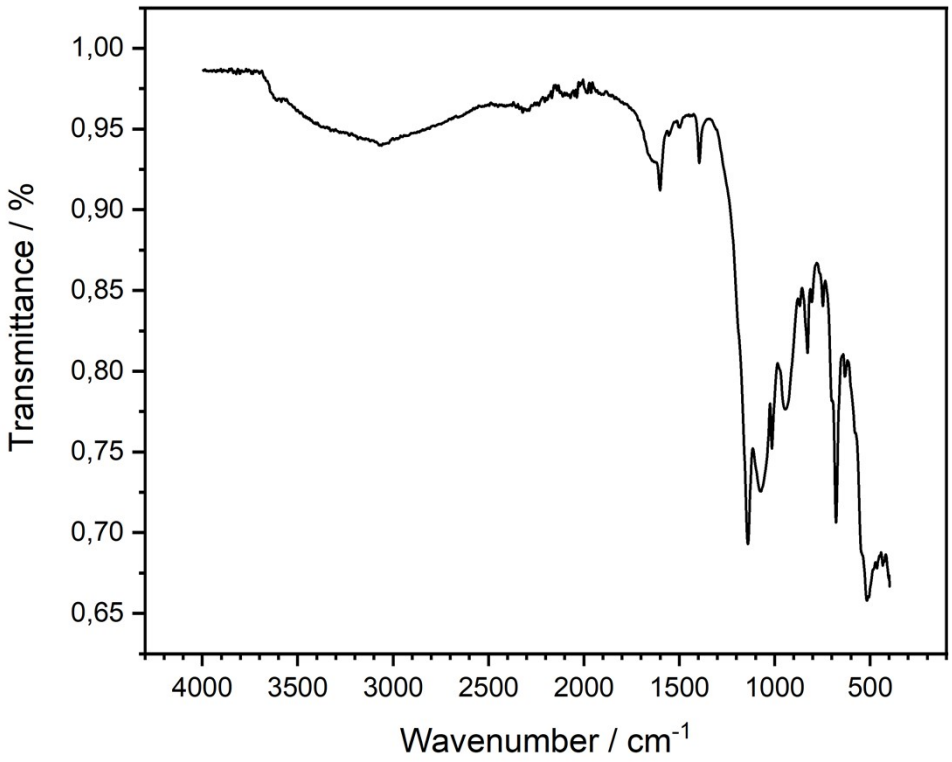

Fig. S31 MIR-spectrum of **Al-CAU-53**.

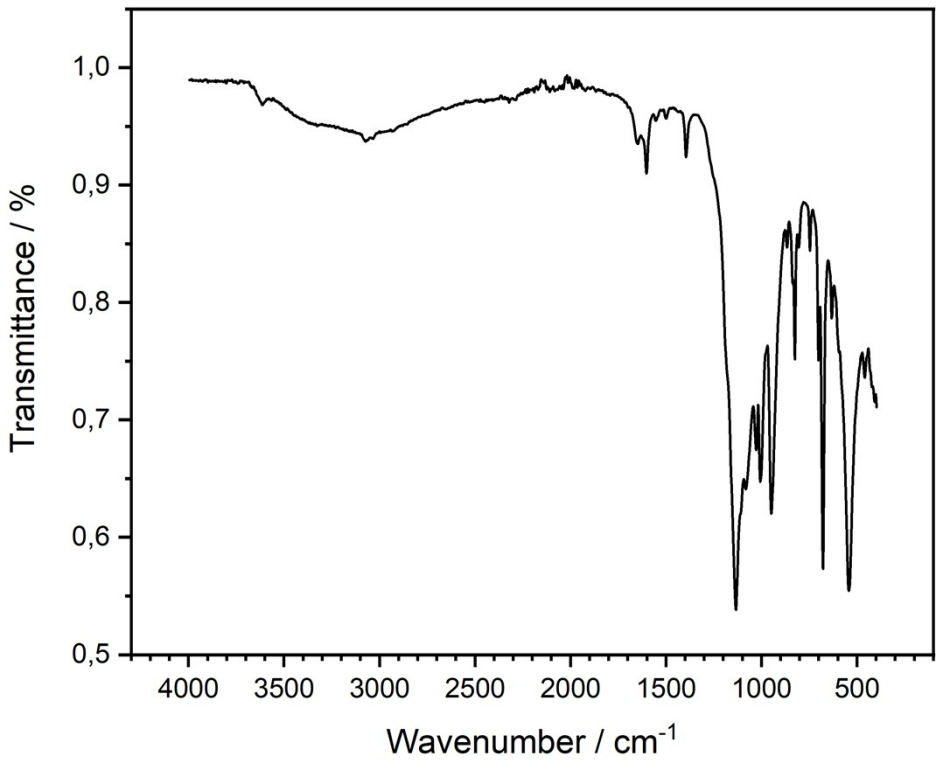

Fig. S32 MIR-spectrum of **Ga-CAU-53**.

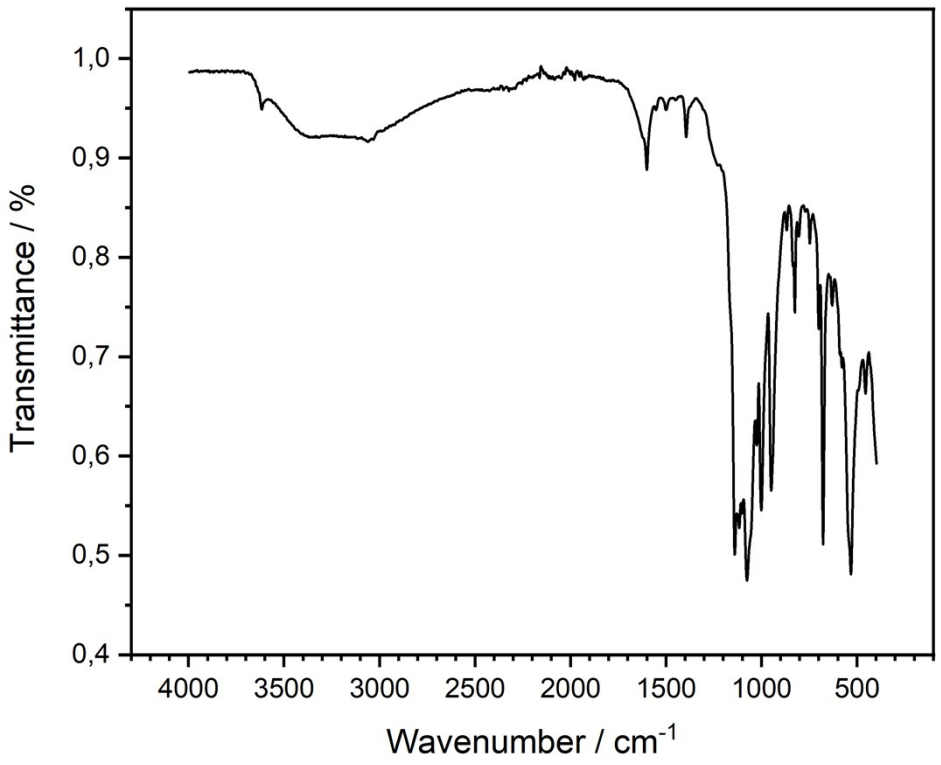

Fig. S33 MIR-spectrum of **Fe-CAU-53**.

6 Impedance spectroscopy

Since the structures of the title compounds feature non-coordinating P-OH groups and therefore could conduct protons as part of an acidic chain, the proton conductivity of **Ga-** and **Fe-CAU-53** was measured. Figure S34 shows the Nyquist plots at different setpoints of relative humidity while Figure S35 shows the Nyquist plots at different setpoints of temperature. The proton conductivity of **Al-CAU-53** was not measured, since it was not possible to produce the compound in a sufficient amount for the measurements.

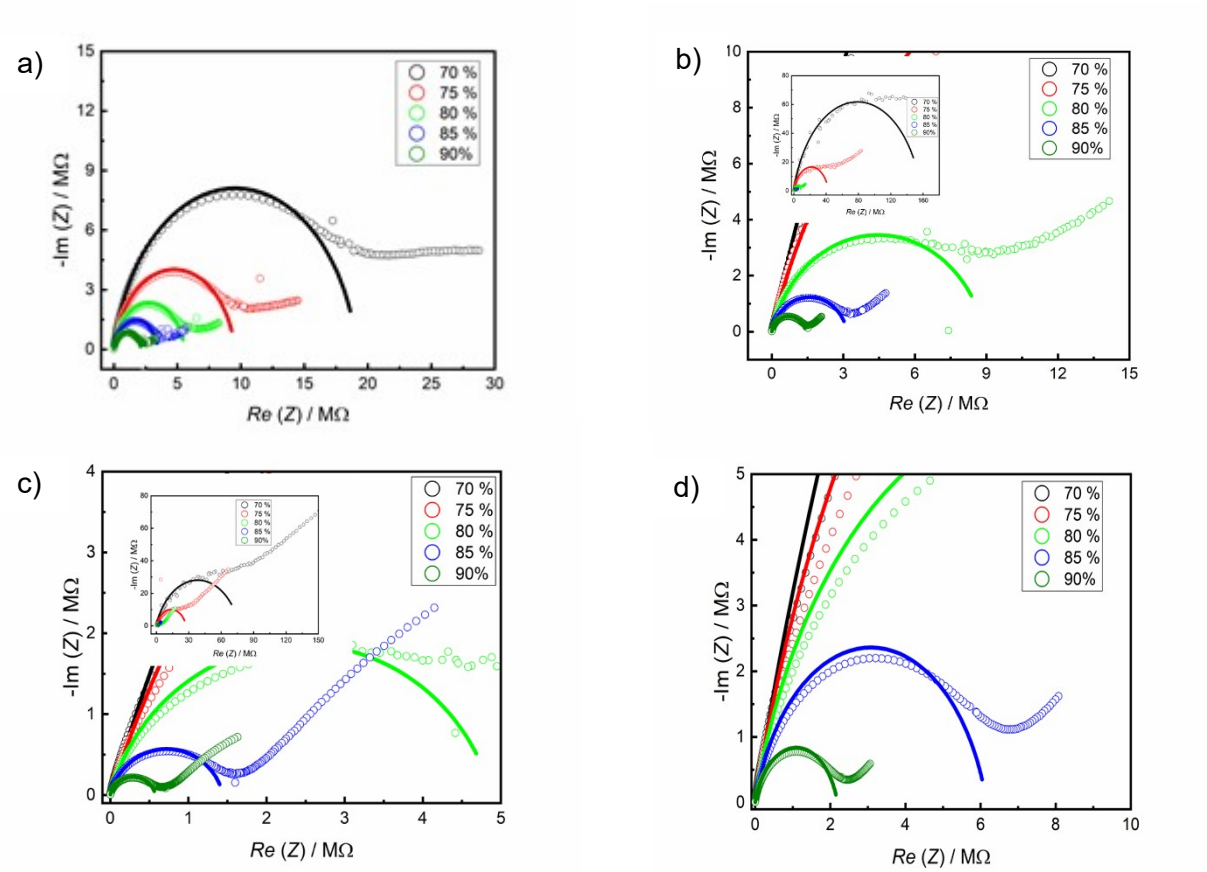

Figure S34: Nyquist plots at several setpoints of relative humidity (temperature 22 °C) (a)- **Ga-CAU-53**$_{as\_snythesized}$; (b)- **Ga-CAU-53**$_{activated}$; (c)- **Fe-CAU-53**$_{as\_synthesized}$; (d)- **Fe-CAU-53** $_{activated}$.

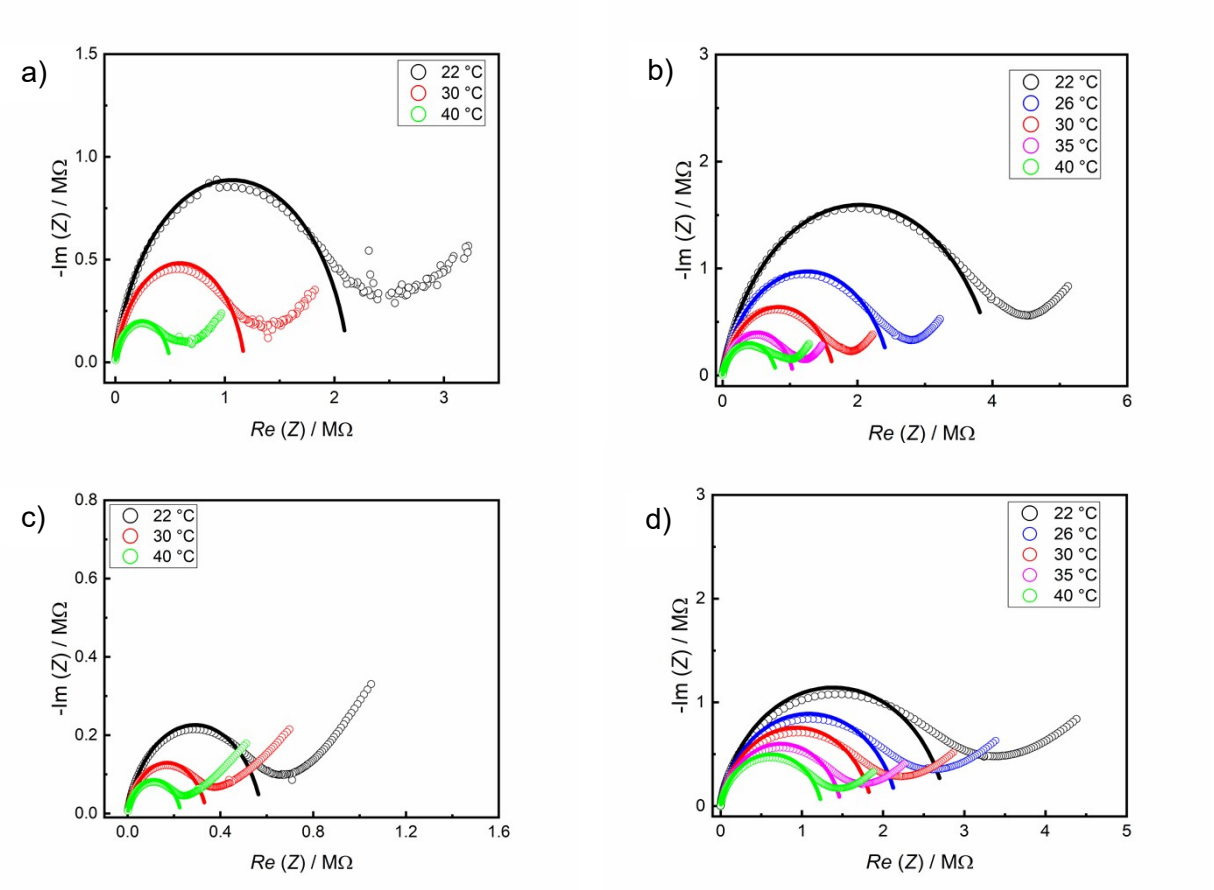

Figure S35: Nyquist plots at several setpoints of temperature (relative humidity 90 %) (a)- **Ga-CAU-53**$_{as\_snythesized}$; (b)- **Ga-CAU-53** $_{activated}$; (c)- **Fe-CAU-53**$_{as\_synthesized}$; (d)- **Fe-CAU-53** $_{activated}$.

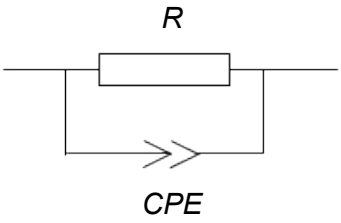

Figure S36: Equivalent circuit model used to fit the semi-circle at high frequency region.

7 Literature

[1] S. Wöhlbrandt, C. Meier, H. Reinsch, E. Svensson Grape, A. K. Inge, N. Stock, *Inorg. Chem.* **2020**, *59*, 13343.

[2] V. Favre-Nicolin, R. Černý, *J. Appl. Crystallogr.* **2002**, *35*, 734.

[3] Accelrys Incorporated, *Materials Studio*, San Diego, **2009**.

[4] H. M. Rietveld, *Acta Cryst.* **1967**, *22*, 151.

[5] A. A. Coelho, *J. Appl. Crystallogr.* **2018**, *51*, 210.

[6] R. A. Coxall, S. G. Harris, D. K. Henderson, S. Parsons, P. A. Tasker, R. E. P. Winpenny, *J. Chem. Soc., Dalton Trans.* **2000**, 2349.

[7] Anthony K. Cheetham, C. N. R. Rao, Russell K. Feller, *Chem. Commun.* **2006**, 4780.

[8] V. A. Blatov, A. P. Shevchenko, D. M. Proserpio, *Cryst. Growth Des.* **2014**, *14*, 3576.

[9] a) O. Delgado-Friedrichs, M. O'Keeffe, *Acta Crystallogr. A: Found. Crystallogr.* **2003**, *59*, 351; b) O. Delgado-Friedrichs, *Gavrog*, http://www.gavrog.org/

[10] a) The Samara Topological Data Center, "topcryst", can be found under https://topcryst.com/ CSD Entry code FITSOR; b) N. Stock, N. Guillou, J. Senker, G. Frey, T. Bein, *Z. anorg. allg. Chem.* **2005**, *631*, 575.